RSC Advances

ROYAL SOCIETY OF CHEMISTRY

www.rsc.org/advances

Porous Ceramic Hollow Fiber-Supported Pebax/PEGDME Composite Membrane for CO_2 Separation from Biohythane

Jun Cheng*, Leiqing Hu, Chaofan Ji, Junhu Zhou, Kefa Cen

State Key Laboratory of Clean Energy Utilization, Zhejiang University, Hangzhou 310027, China

Abstract

To upgrade the mixed gas of fermentative hydrogen and methane for the preparation of biohythane as a gaseous fuel for vehicles, a composite membrane of poly (amide-b-ethylene oxide) (Pebax® MH 1657) and polyethylene glycol dimethylether (PEGDME) coated on porous ceramic hollow fiber was originally proposed for CO_2 separation. The Pebax/PEGDME selective layer with high CO_2 selectivity was closely adhered and evenly distributed to the porous ceramic hollow fiber as a highly permeable support. The ideal CO_2/H_2 selectivity of the composite membrane increased from 12±0.7 to 26±1.7 when the temperature decreased from 50 °C to 10 °C. Competitive sorption between different gas molecules was found in the composite membrane. The fast diffusion of small molecular gas (H_2) through the nanopores in the selective layer improved the diffusion of relatively large molecular gases (CO_2 and CH_4) in the gas mixture. On the contrary, the slow diffusion of large molecular gas (CH_4) worsened the diffusion of relatively small molecular gases (CO_2 and H_2).

Keywords: CO_2 separation, composite membrane, porous ceramic hollow fiber,

* Corresponding author: Prof. Dr. Jun Cheng, State Key Laboratory of Clean Energy Utilization, Zhejiang University, Hangzhou 310027, China. Tel.: +86 571 87952889; fax: +86 571 87951616. E-mail: juncheng@zju.edu.cn

Pebax/PEGDME selective layer, biohythane.

1. Introduction

The use of hydrogen and methane as clean alternative energy sources answers the increasing demand for fossil fuels and reduces the emissions of carbon dioxide and pollutants generated by fossil fuel utilization. Studies have shown that hydrogen-enriched natural gas (HCNG) could solve the problems of natural gases when they are used in automobile engines. Such problems include large cycle-by-cycle variation, poor lean-burn capability, and low thermal efficiency [1, 2]. Moreover, HCNG has shown better combustion characteristics at a methane/hydrogen volume ratio of 4:1 [3]. Among the utilization patterns of biomass energy, the fermentation process of hydrogen and methane cogeneration has shown higher potential [4, 5]. Approximately 40 vol% carbon dioxide is present in biomethane, biohydrogen, and their mixture (mixed according to the 4/1 volume ratio of methane/hydrogen) called biohythane. As a result, the calorific value of these three mixed gases is greatly reduced, thereby resulting in the inefficiency of the direct combustion. Therefore, carbon dioxide separation from these mixed gases is imperative.

Compared with conventional carbon dioxide separation processes that are highly energy intensive, the membrane technology shows great potential because it is compact, portable, environment friendly, has a high energy efficiency, and simpler mode of operation [6]. Dense polymeric membranes have been widely used for gas separation purposes, and the dominant transport mechanism of solution-diffusion

governs the transport of the penetrating gases [7]. This result indicates that different gas molecules have different solubilities and diffusivities as they pass through these membranes. Moreover, the solubility (based on the chemical properties of gases and membranes) enable these membranes to separate larger gas molecules from smaller ones. During carbon dioxide separation from the fermentation of hydrogen and methane, the use of CO_2-philic dense polymeric membranes with very high CO_2/H_2 selectivity and CO_2/CH_4 selectivity could separate CO_2 in one step and avoid the recompression of H_2 and CH_4 [8], as well as reduce the loss of H_2 and CH_4. Therefore, CO_2-philic polymers with high CO_2 permeability and selectivity are adopted to achieve CO_2 separation from fermentation gases [7].

In a recent review on the influence of primary chemical structure on CO_2-philic polymers, ethylene oxide (EO) units have been identified as the best chemical groups for such membranes because the polar ether oxygens in the EO units interacted favorably with carbon dioxide, and the polymers containing EO could be highly flexible, leading to a weak size-sieving behavior and high diffusion coefficients, two factors that contribute directly to high CO_2 permeability and selectivity [8, 9]. Among the polymers containing EO units, Pebax, $HO[(C_2H4O)_xCO(NHC_5H_{10}CO)_y]_nOH$, has been considered as a promising membrane material [10]. Pebax is a co-polymer consisting of polyamide (PA) as the hard segment that provides mechanical strength and poly (ethylene oxide) (PEO) that is responsible for the gas separation properties of the membrane [11]. . Moreover, many studies have shown that the incorporation of poly (ethylene glycol) (PEG)-based polymers (PEGs) into Pebax improved CO_2

permeability and selectivity. For example, Wilfredo Yave and Anja Car [11-13] prepared Pebax/PEG200 dense films and PAN-supported composite membranes. At 30 °C, the highest ideal CO_2/H_2 selectivity of dense films reached 10.8. Moreover, the composite membranes obtained the ideal CO_2/CH_4 selectivity of about 16. They [14] also prepared Pebax/PEGDME films. At 30 °C, a maximum CO_2/H_2 selectivity of 15.2 and a maximum CO_2 permeability of 606 Barrers (1 Barrer = 1×10^{-10} cm^3(STP) •μm / (cm^2•s•cmHg), where STP is the standard temperature and pressure) were obtained. Md. Mushfequr Rahman [15] prepared nanocomposite membranes by incorporating PEG-functionalized POSS in two grades of Pebax, and the CO_2/H_2 selectivity was about 10 at 30 °C. Shaofei Wang [16] prepared Pebax/PEGs membranes and obtained a CO_2 permeability of 553 Barrers at room temperature.

To date, most Pebax/PEGs membranes reported for carbon dioxide separation have shown good permeation and separation performance. However, these membranes, which are free-standing or supported by a porous polymer, suffered from low mechanical, chemical, and thermal stability [17]. As a new support, porous ceramic hollow fibers have drawn increasing attention from researchers because of several advantages listed below: (1) As one type of ceramic supports, it could provide sufficient mechanical stiffness to support a thin selective layer even at a high pressure [17]; (2) High packing density and area/volume ratio. Membrane surface area/volume ratio > 1000 m^2/m^3, if the outer diameter is smaller than 4 mm [18]. (3) The low transport resistance of the porous hollow fiber could enhance the gas permeability. (4) The rigid ceramic supports could confine the polymer that penetrated into the pores.

Thus, the stability of the composite membrane is improved with the confinement effect [17].

In the present work, porous ceramic hollow fibers were first used to support CO_2-philic polymer selective layers. Pebax/PEGDME (the mass ratio was 50:50) were adopted as CO_2-philic polymer materials and the ceramic hollow fiber-supported Pebax/PEGDME composite membrane was prepared via coating method. The permeation and separation performance of this composite membrane was investigated at different temperatures.

2. Experimental

2.1. Materials

Pebax® MH 1657, containing 60 wt% poly (ethylene oxide) (PEO) and 40 wt% polyamide 6 (PA6), was provided by Arkema Company [16]. Poly (ethylene glycol) dimethyl ether (PEGDME) (average M.W. _500) was obtained from Sigma-Aldrich Company. The molecular structure of PEGDME was $CH_3O(C_2H_4O)_nCH_3$ [7]. Asymmetric α-Al_2O_3 ceramic hollow fibers (internal diameter was about 1 mm, external diameter was about 1.4 mm, average pore size of outside layer was 200 nm, and porosity was about 60%) were provided by the State Key Laboratory of Chemical Engineering at Zhejiang University, China. Torr seal was bought from Shanghai Passion Auto & Tec Company.

2.2. Preparation of Pebax/PEGDME coating solution

The preparation method of Pebax/PEGDME solution was similar to that of another report [14]. About 4 g of Pebax MH 1657 pellets was dissolved in 76 g of the solvent mixture consisting of 70/30 (weight ratio) ethanol/water. The polymer solution was stirred under reflux at 80 °C for 2 h until it was completely dissolved. After cooling the solution to room temperature, 4 g of PEGDME was added and the solution was stirred for 1 h at room temperature. Finally, the obtained homogeneous solution was filtered through a stainless steel filter with a pore size of 32 μm.

2.3. Fabrication of composite membranes

The composite membranes were fabricated via a two-time dip coating method. First, one end of the ceramic hollow fiber was inserted and attached to a stainless steel capillary. Another end was sealed with Torr seal. The effective area of the ceramic hollow fiber was 0.79 cm^2. After pre-wetted by de-ionized water for about 10 s, the ceramic hollow fiber was immersed into the Pebax/PEGDME coating solution for 20 s. The viscosity of the coating solution was 13.2 mPa**.**s. The hollow fiber was then dried at 80 °C for 2 h. The hollow fiber was then immersed again into the coating solution for another 20 s. The viscosity of the coating solution increased to 21.8 mPa**.**s because the solution slowly crystallized. Finally, the composite hollow fiber was dried at 313 K for 15 h and at 293 K for 5 d before testing the gas separation performance.

2.4. Membrane characterization

The morphology of the ceramic-supported Pebax/PEGDME composite membrane was observed using a Hitachi SU-70 field emission scanning electron microscope (FESEM, FEG650, FEI, Holland) operated at 3 kV. Before analysis, the membranes were cryogenically fractured in liquid nitrogen and then sputtered with a thin layer of gold.

2.5. Gas permeation experiments

Three membranes had been successively fabricated under the same conditions. The data were average values of these three membranes measured in the same conditions. Gas permeation measurements were conducted at different temperatures to evaluate the gas separation performance of the composite membranes. All feed pressures and flow rates of feed gases were 0.12 MPa and 100 sccm, respectively. Pure component gases, such as CO_2, H_2, and CH_4, and three gas mixtures, namely, biohydrogen (40 vol% CO_2, 60 vol% H_2), biomethane (40 vol% CO_2, 60 vol% CH_4), and biohythane (48 vol% CH_4, 40 vol% CO_2, 12 vol% H_2) were used as the feed gases. Ar was employed as the sweep gas and was kept at atmospheric pressure and temperature. The flow rate of sweep gas was 2 sccm. The flow rate of the individual gases was controlled using mass flow controllers (Seven Star, CS200C, China). The operating temperature was measured by a thermometer and controlled using a constant low–temperature bath (Hangzhou David science instrument co., GDC1015, China). The bath was heated or cooled to the setting temperature before membrane

separation device was put into the bath. The composition of the permeate gas was analyzed using a gas chromatograph (Agilent, 7820A, USA). The gas permeability and selectivity were calculated according to equations 1–3 [19, 20]:

$$P = D \bullet S \quad (1)$$

$$J = P / L = Q / S_m \Delta p \quad (2)$$

$$\alpha_{A/B} = J_A / J_B \quad (3)$$

where P is the gas permeability coefficient. The unit of P is Barrer. D is the diffusivity and S is the solubility. J is the gas permeation rate, which indicates the permeability of a single gas or a component in a mixture when the thickness of the selective layer is unknown or difficult to measure. The unit of J is GPU (1 GPU=1×10^{-6} cm^3(STP)/(cm^2•s•cmHg)). L is the thickness of the selective layer. Q is the gas flow rate. S_m is the effective permeation area of composite membrane. Δp is the pressure difference across the membrane. The gas selectivity $\alpha_{A/B}$ is the ratio of J_A and J_B, which are the permeation rates of gases A and B, respectively.

3. Results and discussion

3.1. Membrane characterization

To observe the surface changes of porous ceramic hollow fiber after adding the Pebax/PEGDME selective layer and the cross-section of the composite membrane, SEM analyses were carried out. Figs. 1 (a) and (b) show the surface of the ceramic hollow fiber support and the ceramic hollow fiber-supported Pebax/PEGDME composite membrane, respectively. Macropores with an average diameter of 200 nm

are uniformly distributed between Al_2O_3 particles (Fig.1 (a)). The porous surface of the support is covered by a dense and defect-free surface after coating the polymer selective layer. Numerous particulate matters with diameters ranging from 1 μm to 5 μm are observed on the surface of the Pebax/PEGDME selective layer (Fig.1 (b)). This result is due to the polymer Pebax® MH 1657 containing 40 wt% crystralline polyamide (polyamide 6), which contributes to the existence of large particle structures [15]. Meanwhile, the agglomeration of polymers in the coating solution probably happens during the time interval between the first and second coating of the ceramic hollow fiber caused by the intrinsic van derWaals force [21]. The cross-section image (Fig.1 (c)) reveals that the Pebax/PEGDME selective layer closely adheres on the support with no gap in the cross section. Given that the support was pre-wetted by de-ionized water before coating the selective layer, no obvious interface layer is formed by the penetration of the polymer solution into the ceramic support. Therefore, the gas permeability is improved. Fig.1 (c) reveals that the thickness of Pebax/PEGDME selective layer is approximately 25 μm. It is proved by several other cross-section images obtained by SEM. These observations are similar to those reported previously, and the differences could be attributed to the preparation method because the polymer-solvent system is the same [12].

3.2. CO_2 gas permeability and competitive sorption mechanism

For the porous ceramic hollow fiber supported composite membrane, the permeability and selectivity are determined by the Pebax/PEGDME selective layer.

The gas permeation of the dense selective layer is based on the transport mechanism of solution-diffusion, as represented in Eq. (1). Gas permeability involves solubility and diffusivity. In the selective layer, the selectivity (α) of a pair of gases can also be described as Eq.(4) [8].

$$\alpha_{A/B} = \left(\frac{D_A}{D_B}\right)\left(\frac{S_A}{S_B}\right) \qquad (4)$$

where D_A/D_B is the diffusivity selectivity and S_A/S_B is the solubility selectivity. The primary factor influencing diffusivity is the kinetic diameter of the penetrating gas molecule. A small kinetic diameter indicates a high diffusivity. The kinetic diameters of H_2, CO_2, and CH_4 molecules are 2.89, 3.30, and 3.82 Å (1 Å=10^{-10} m), respectively [21]. Therefore, $D_{H_2}>D_{CO_2}>D_{CH_4}$, $D_{CO_2}/D_{H_2}<1$. The gas solubility is enhanced by increasing the condensability of the gas molecules. A high critical temperature of gas molecules indicates good condensability. The critical temperatures of H_2, CO_2, and CH_4 are 33.2 K, 304.2 K, and 190.6 K [21], respectively; thus, carbon dioxide has the best solubility and H_2 has the worst solubility. As rubbery polymers, both Pebax and PEGDME weakened the diffusivity selectivity and enforced the solubility selectivity [8]. Consequently, the permeability of CO_2 is much higher than those of other gases.

Fig. 2 shows the CO_2 permeation rates in pure and mixed gases as they pass through the porous ceramic hollow fiber supported Pebax/PEGDME composite membrane at different operating temperatures. The highest permeation rate (35.69±0.84 GPU) is obtained at 50 ºC. The comparison of CO_2 permeation rates between gases containing different components is as follows: $J_{biomethane} < J_{biohythane} \approx$

$J_{pure\ CO_2} < J_{biohydrogen}$. Furthermore, the CO_2 permeation rates in biohydrogen are always higher 35% than that in biomethane. Moreover, the difference has a great effect on CO_2 separation from fermentation gases. The phenomenon above can be explained by competitive sorption between penetrating gas molecules, as Fig. 3. It is known, for instance, that the presence of a "slow" gas can reduce the permeability of a "fast" gas; conversely, the presence of a fast gas increases the permeability of a slow gas [22, 23]. For the Pebax/PEGDME selective layer, the competition is mainly reflected in the diffusivity. In other words, relative to CO_2, H_2 is a fast gas in terms of diffusivity, and the competition between CO_2 and H_2 molecules is weaker than that between CO_2 molecules themselves. Therefore, the existence of H_2 in biohydrogen optimizes the permeation condition of CO_2 in the composite membrane, thereby resulting in an increase in the CO_2 permeation rate. However, among CO_2, H_2, and CH_4, CH_4 is the slowest gas in terms of diffusivity. As a result, the competition between CO_2 and CH_4 molecules is more drastic than that between CO_2 molecules themselves. Hence, the CO_2 permeability decreases because of the existence of 60% CH_4 in biomethane. Moreover, for CO_2 permeation in biohythane, the deterioration of CH_4 offsets the optimization of H_2. Therefore, the difference of CO_2 permeation rates between pure CO_2 and biohythane is relatively small.

The effect of operating temperature on CO_2 permeability as the gas passes through the composite membrane is also shown in Fig. 2. The CO_2 permeation rates in all gases almost increase linearly with increasing temperature. The result is similar with those of another study [15]. Specifically, taking pure CO_2 as an example, when the

operating temperature was from 10 ºC to 50 ºC, the CO_2 permeation rate increases from 11.78±0.4 GPU to 31.1±1.95 GPU. The growth rate is nearly triple. Two main factors are considered to explain the considerable increase in the permeation rate. On one hand, the thermodynamic energy of CO_2 molecules is improved with increasing temperature. Therefore, the mobility of CO_2 molecules increases, which enhances the driving force for diffusion. On the other hand, the increase in the operating temperature leads to more flexible polymer chains, thereby creating more free volume cavities for molecule transport [16]. In addition, the difference in the CO_2 permeation rates between biohythane and biomethane is enlarged with increasing temperature, where a difference of about 4 GPU at 10 ºC increases to 9 GPU at 50 ºC. Competitive sorption between gas molecules is probably intensified by the elevated operating temperature, thereby contributing to the phenomenon described above.

3.3. H_2 gas permeability and CO_2/H_2 selectivity

Fig. 4 shows the change in the H_2 permeation rates for the component difference of gases. The change trend is as follows: $J_{pure\ H2} < J_{biohythane} < J_{biohydrogen}$. At 20 ºC, for example, $J_{pure\ H2}$ is 0.81±0.09 GPU, $J_{biohythane}$ is 0.95±0.04 GPU, and $J_{biohydrogen}$ is 1.16±0.04 GPU. The H_2 permeation rates in biohydrogen are always higher about 40% than that in pure hydrogen. CO_2-induced plasticization on the polymer membranes can account for this phenomenon. In the Pebax/PEGDME selective layer, the strong sorption of CO_2 results in an enhancement of the local segmental mobility of the polymer chains, for which the transport resistance of H_2 was reduced [24, 25]. The effects

of CO_2-induced plasticization on permeability of H_2 in biohydrogen were measured for consecutive 7 days. The experiments were conducted at operating temperature of 30 °C for two hours every day. The permeation rate of H_2 measured every day was nearly consistent of 1.6 GPU and the deviations of experimental data were less than ±5%. Therefore, the performance of membranes with CO_2-induced plasticization can be almost recovered after CO_2 permeation experiments. However, relative to CO_2, CH_4 in biohythane causes the permeability of H_2 to decrease more significantly. Consequently, H_2 in biohydrogen allows for the best condition for permeation. Furthermore, the H_2 permeation rates significantly increased with increasing operating temperature, and a six-fold increase is observed in pure hydrogen. The reasons for this increase are the enhancement of the mobility of gas molecules and the increase in the fractional free volume.

As shown in Fig. 4, the CO_2/H_2 selectivity decreases with increasing operating temperature. Specifically, the ideal CO_2/H_2 separation factor increases to 26±1.7 at 10 ºC, which is more than two times of 12±0.7 at 50 ºC. The solubility selectivity increases at a low temperature because the CO_2 solubility is enhanced by increased affinity and interaction between CO_2 molecules and PEO segments in Pebax and PEGDME [20]. Meanwhile, the gas diffusivity selectivity decreases with decreasing operating temperature [24]. In biohydrogen, CO_2 and H_2 improve each other's permeability for induced plasticization and competitive sorption. But the improvement in H_2 permeability is more significant at low temperatures. Therefore, the CO_2/H_2 selectivity in biohydrogen is lower than the ideal CO_2/H_2 selectivity.

Furthermore, the positive effect of increasing operating temperature is most significant on the permeation rate of pure hydrogen. Therefore, the decrease in the ideal CO_2/H_2 selectivity is faster than the decrease in the CO_2/H_2 selectivity in biohydrogen. Moreover, the competitive sorption between a big gas molecule and another big gas molecule (such as CH_4 and CO_2) is probably more serious than that between a big gas molecule and a small gas molecule (such as CH_4 and H_2). Therefore, relative to H_2, CO_2 suffers from a greater loss of permeation rate from the competitive sorption of methane in biohythane. As a result, the CO_2/H_2 selectivity is relatively at the minimum.

3.4. CH_4 gas permeability and CO_2/CH_4 selectivity

The effects of operating temperature and gas composition on CH_4 permeation rate is shown in Fig. 5. Given the elevated temperature, the reason for the increase in CH_4 permeation rate is similar to the reasons for the increase in H_2 permeation rate. Among pure methane, biomethane, and biohythane, the CH_4 permeation rate in pure methane is the lowest. Specifically, at a high operating temperature, the difference in the CH_4 permeation rates between pure methane and the other two mixed gases increases. This result is probably due to the positive effect of CO_2-induced plasticization on the permeability of the large CH_4 molecules, and this effect becomes more apparent at high temperatures.

From Fig. 5, the ideal CO_2/CH_4 selectivity is the largest, followed by the CO_2/CH_4 selectivity in biohythane. The CO_2/CH_4 selectivity in biomethane is the

lowest. Meanwhile, with the temperature increased from 10 ºC to 50 ºC, the values of CO_2/CH_4 selectivity decreased by around 50%. Both the increase in temperature and CO_2-induced plasticization increased the mobility of the polymer segment. The increase in local segmental mobility results in enhanced transport rates of CO_2 and CH_4. Given that the transport rate of the 'slow' component (CH_4) is more affected than that of a 'fast' component (CO_2), plasticization and increase in the operating temperature typically result in a loss of membrane selectivity [25]. Moreover, given that the existence of H_2 in biohythane weakens the deterioration of CO_2 permeability imposed by CH_4, the CO_2/CH_4 selectivity in biohythane is higher than that in biomethane.

3.5. Comparison of CO_2/H_2 separation performance with other literatures

During the engineering application of membrane separation for biohythane upgrading, a high CO_2/H_2 selectivity is of great importance to ensure the recovery of hydrogen. Table.1 shows the CO_2/H_2 selectivities of Pebax/PEGs gas separation membranes in recent studies. Porous ceramic hollow fiber-supported Pebax/PEGDME composite membrane has a higher CO_2/H_2 selectivity compared to other Pebax/PEGs membranes. The following two points can explain well the selectivity advantage of the membrane. First, given that the surface of the porous ceramic hollow fiber is rough and pre-wetted by deionized water before dip coating, the Pebax/PEGDME coating solution is confined to the surface of the ceramic hollow fiber. Meanwhile, the two-time dip coating method was adopted. Therefore, an even selective layer is

formed on the surface of the porous ceramic hollow fiber, and the degradation of membrane selectivity caused by the uneven distribution of membrane thickness is reduced. Second, the Pebax/PEGDME selective layer has high CO_2 solubility and solubility selectivity, especially when incorporated with 50% PEGDME, which significantly improves the whole performance of the selective layer [14].

4. Conclusion

Composite membranes with the Pebax/PEGDME selective layer that evenly adhered on a porous ceramic hollow fiber could separate CO_2 efficiently from biohythane. The ideal CO_2/H_2 separation factor increased to 26±1.7. Given the existence of competitive sorption, H_2 increased the permeability of CO_2 and CH_4, whereas CH_4 decreased the permeability of H_2 and CO_2. Meanwhile, CO_2-induced plasticization on polymer chains increased the permeation rates of H_2 and CH_4. Increasing the operating temperature enhanced the gas permeability of the composite membrane but worsened CO_2 separation. To further increase the CO_2 separation efficiency from biohythane, the CO_2/CH_4 selectivity of the porous ceramic hollow fiber-supported Pebax/PEGDME composite membrane should be continuously improved in the future.

Acknowledgments

This study was supported by the National Science Foundation-China (51176163, 51476141), National High Technology R&D Program-China (2012AA050101), Zhejiang Provincial Natural Science Foundation-China (LR14E060002), Program of

Introducing Talents of Discipline to University-China (B08026).

References

1. J. Deng, F. H. Ma, S. Li, Y. T. He, M. Y. Wang, L. Jiang and S. L. Zhao, *Int J Hydrogen Energ*, 2011, **36**, 13150-13157.
2. E. J. Hu, Z. H. Huang, B. Liu, J. J. Zheng and X. L. Gu, *Int J Hydrogen Energ*, 2009, **34**, 1035-1044.
3. F. H. Ma, Y. F. Wang, S. F. Ding and L. Jiang, *Int J Hydrogen Energ*, 2009, **34**, 6523-6531.
4. B. F. Xie, J. Cheng, J. H. Zhou, W. L. Song and K. F. Cen, *Int J Hydrogen Energ*, 2008, **33**, 5006-5011.
5. J. Cheng, R. C. Lin, L. K. Ding, W. L. Song, Y. Y. Li, J. H. Zhou and K. F. Cen, *Bioresource Technol*, 2015, **179**, 407-413.
6. J. E. Ramirez-Morales, E. Tapia-Venegas, N. Nemestothy, P. Bakonyi, K. Belafi-Bako and G. Ruiz-Filippi, *Int J Hydrogen Energ*, 2013, **38**, 14042-14052.
7. M. K. Barillas, R. M. Enick, M. O'Brien, R. Perry, D. R. Luebke and B. D. Morreale, *J Membrane Sci*, 2011, **372**, 29-39.
8. H. Q. Lin, E. Van Wagner, B. D. Freeman, L. G. Toy and R. P. Gupta, *Science*, 2006, **311**, 639-642.
9. H. Q. Lin, B. D. Freeman, S. Kalakkunnath and D. S. Kalika, *J Membrane Sci*, 2007, **291**, 131-139.
10. P. Bernardo, J. C. Jansen, F. Bazzarelli, F. Tasselli, A. Fuoco, K. Friess, P. Izak, V. Jarmarova, M. Kacirkova and G. Clarizia, *Sep Purif Technol*, 2012, **97**, 73-82.
11. A. Car, C. Stropnik, W. Yave and K. V. Peinemann, *J Membrane Sci*, 2008, **307**, 88-95.
12. A. Car, C. Stropnik, W. Yave and K. V. Peinemann, *Sep Purif Technol*, 2008, **62**, 110-117.
13. W. Yave, A. Car, K. V. Peinemann, M. Q. Shaikh, K. Ratzke and F. Faupel, *J Membrane Sci*, 2009, **339**, 177-183.
14. W. Yave, A. Car and K. V. Peinemann, *J Membrane Sci*, 2010, **350**, 124-129.
15. M. M. Rahman, V. Filiz, S. Shishatskiy, C. Abetz, S. Neumann, S. Bolmer, M. M. Khan and V. Abetz, *J Membrane Sci*, 2013, **437**, 286-297.
16. S. F. Wang, Y. Liu, S. X. Huang, H. Wu, Y. F. Li, Z. Z. Tian and Z. Y. Jiang, *J Membrane Sci*, 2014, **460**, 62-70.
17. S. N. Liu, G. P. Liu, W. Wei, F. J. Xiangli and W. Q. Jin, *Chinese J Chem Eng*, 2013, **21**, 348-356.
18. S. Y. Zhou, X. Q. Zou, F. X. Sun, F. Zhang, S. J. Fan, H. J. Zhao, T. Schiestel and G. S. Zhu, *J Mater Chem*, 2012, **22**, 10322-10328.
19. W. Yave, H. Huth, A. Car and C. Schick, *Energ Environ Sci*, 2011, **4**, 4656-4661.
20. H. Z. Chen, Z. W. Thong, P. Li and T. S. Chung, *Int J Hydrogen Energ*, 2014, **39**, 5043-5053.
21. D. Zhao, J. Z. Ren, H. Li, X. X. Li and M. C. Deng, *J Membrane Sci*, 2014, **467**, 41-47.
22. C. R. Antonson, R. J. Gardner, C. F. King and D. Y. Ko, *Ind Eng Chem Proc Dd*, 1977, **16**, 463-469.
23. W. J. Koros, R. T. Chern, V. Stannett and H. B. Hopfenberg, *J Polym Sci Pol Phys*, 1981, **19**, 1513-1530.
24. P. Bakonyi, N. Nemestothy and K. Belafi-Bako, *Int J Hydrogen Energ*, 2013, **38**, 9673-9687.
25. S. R. Reijerkerk, K. Nijmeijer, C. P. Ribeiro, B. D. Freeman and M. Wessling, *J Membrane Sci*, 2011, **367**, 33-44.
26. L. J. Wang, Y. Li, S. G. Li, P. F. Ji and C. Z. Jiang, *J Energy Chem*, 2014, **23**, 717-725.

List of Figures and Tables:

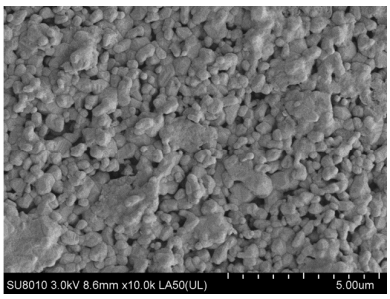

(a)

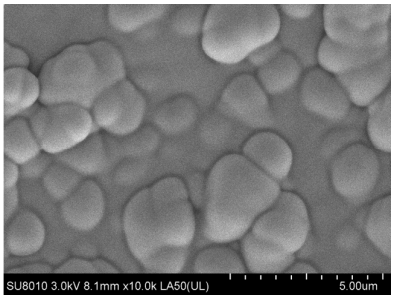

(b)

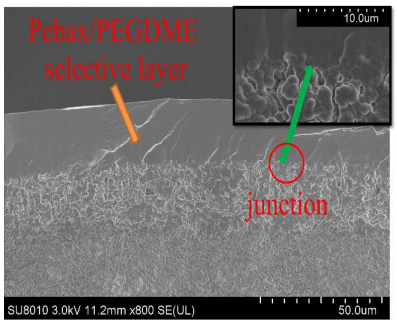

(c)

Fig. 1 SEM images of the surface of ceramic hollow fiber support (a), surface of ceramic hollow fiber-supported Pebax/PEGDME composite membrane (b), and cross-section of the membrane (c)

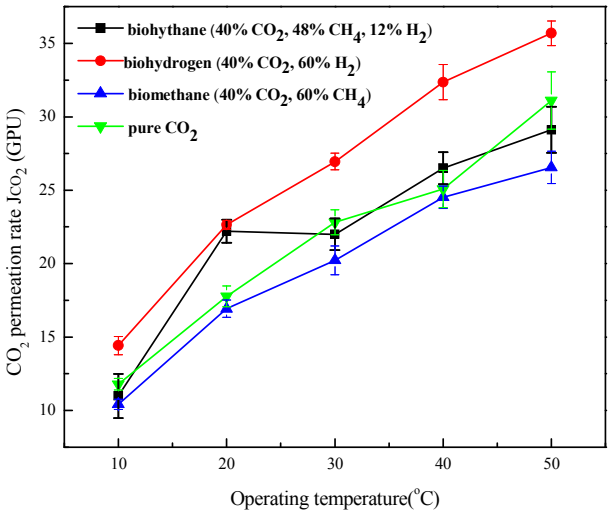

Fig. 2 CO_2 permeation rate (J_{CO_2}) in the porous ceramic hollow fiber-supported Pebax/PEGDME composite membrane (Feed pressures of pure CO_2 and mixed gases were constant at 0.12 MPa)

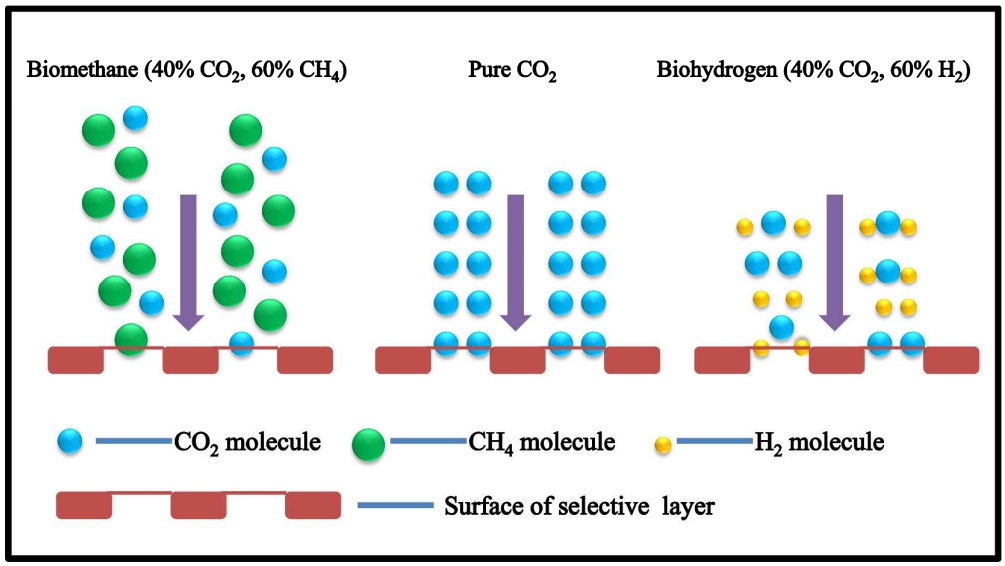

(a)

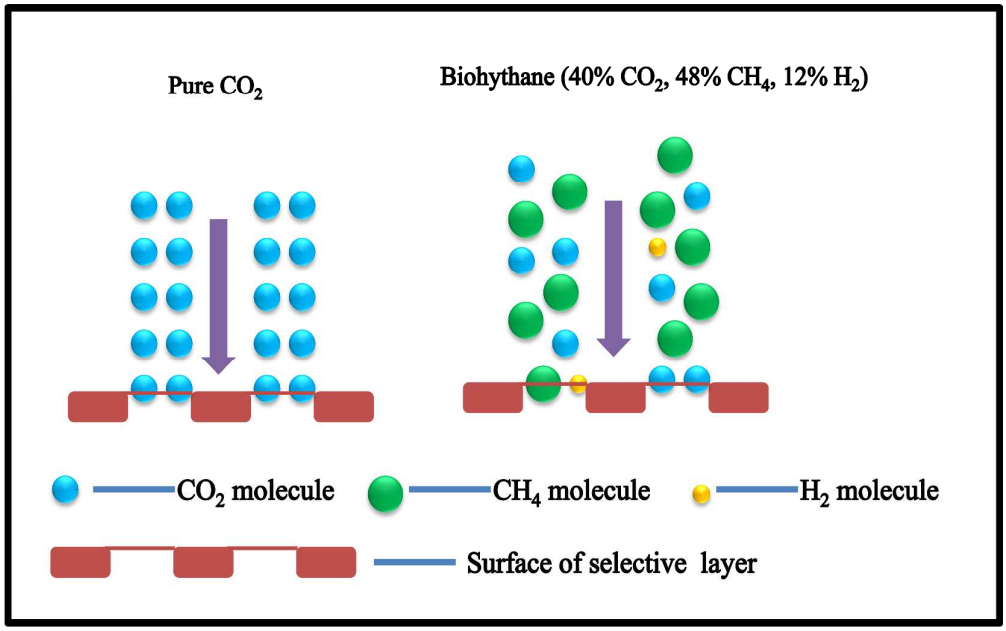

(b)

Fig. 3 Mechanisms of competitive sorption between gas molecules in binary gases (a) and ternary gas (b) during diffusion into the Pebax/PEGDME selective layer

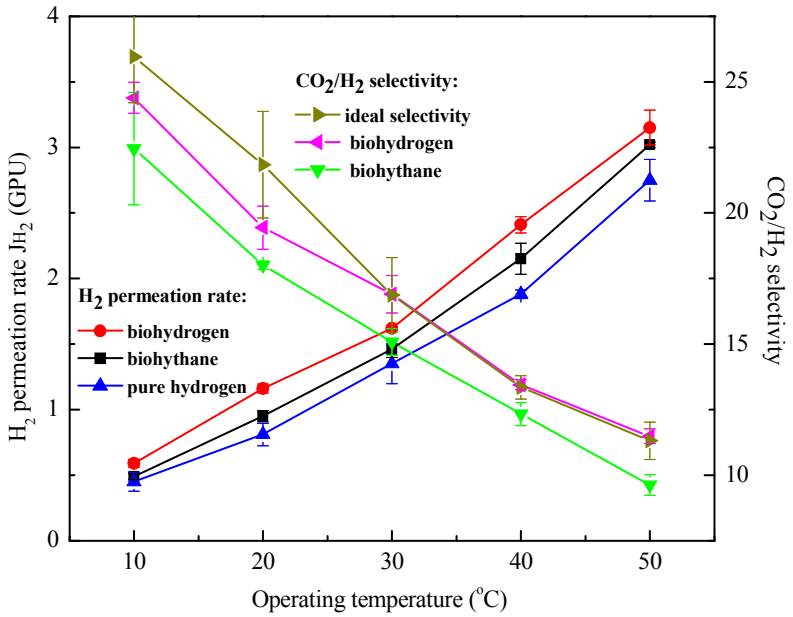

Fig. 4 H_2 permeation rate (J_{H2}) and CO_2/H_2 selectivity in the porous ceramic hollow fiber-supported Pebax/PEGDME composite membrane (Feed pressures of pure or mixed gases were constant at 0.12 MPa)

Note: Biohythane: 40% CO_2, 48% CH_4, 12% H_2; Biohydrogen: 40% CO_2, 60% H_2; Ideal selectivity: Jpure CO_2/Jpure H_2.

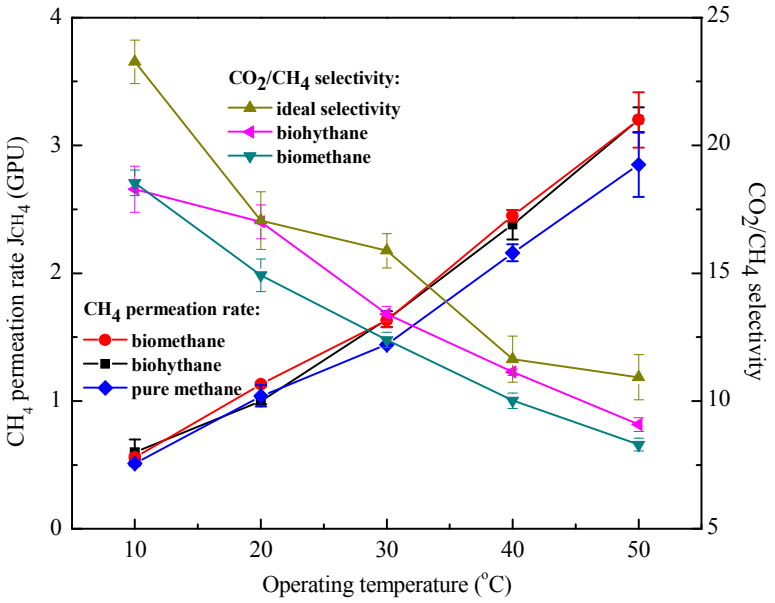

Fig. 5 CH_4 permeation rate (J_{CH4}) and CO_2/CH_4 selectivity in the porous ceramic hollow fiber-supported Pebax/PEGDME composite membrane (Feed pressures of pure or mixed gases were constant at 0.12 MPa)

Note: Biohythane: 40% CO_2, 48% CH_4, 12% H_2; Biomethane: 40% CO_2, 60% CH_4; Ideal selectivity: Jpure CO_2/Jpure CH_4.

Table.1 Comparison of CO_2/H_2 separation performance of Pebax/PEGs membranes between this study and other studies

Material	Configuration of membrane	Testing conditions	Permeability coefficient of CO_2	CO_2/H_2 selectivity	References
Pebax® MH1657/50% PEGDME	film	30 ºC, pure gases, feed pressure: 0.03 MPa	606 Barrers	15.2	14
Pebax® MH1657/50% PEG 200	film	30 ºC, pure gases, feed pressure: 0.06 MPa	151 Barrers	10.8	11
Pebax® MH1657/50% PEG 200	PAN-supported film	30 ºC, pure gases, feed pressure: 0.1 MPa	122 Barrers	9.3	12,13
		20 ºC, mixed gas (50% CO_2, 50% H_2), feed pressure: 0.5 MPa	about 111 Barrers[a]	9.6	
Pebax® MH1657/30% PEG-POSS	film	30 ºC, pure gases, feed pressure: 0.1 MPa	about 190 Barrers	about 12.5	15
Pebax® MH2533/30% PEG-POSS	film	30 ºC, pure gases, feed pressure: 0.1 MPa	about 350 Barrers	about 11	
Pebax® MH1657-40% PEGDME/MWCNT	film	22 ºC, pure gases, feed pressure: 0.1 MPa	about 555 Barrers	--[d]	16
Pebax® MH1657-40% PEG400/MWCNT	film	22 ºC, pure gases, feed pressure: 0.1 MPa	about 341 Barrers	--[d]	
Pebax® MH1657-PEGDME /amino-PDMS	PAN-supported film	20 ºC, pure gases, feed pressure: 0.5 MPa	about 400 Barrers[b]	--[d]	26
PEGDME	Nylon-supported film	37 ºC, mixed gas (20% CO_2,20% H_2,balance Ar), feed pressure: 0.01 MPa	814 Barrers	11.1	7
Pebax® MH1657/50% PEGDME	Ceramic hollow fiber-supported	30 ºC, pure gases, feed pressure: 0.12 MPa	570±21 Barrers[c]	16.9±1.4	This study
		30 ºC, mixed gas (40 % CO_2, 60% H_2), feed pressure: 0.12 MPa	674±14 Barrers[c]	16.9±0.7	

Notes:

a: J was calculated by transforming the unit, the origin data was 31×10^{-2} $m^3/(m^2$ h bar), and the thickness of separating layer was considered as 1 μm;

b: The thickness of the separating layer was considered as 1 μm from the SEM images;

c: P was calculated when the thickness of the separating layer was considered constant as 25 μm;

d: No data.